A Comparison of Suitable Control Methods for Full Vehicle with Four MR Dampers, Part I: Formulation of Control Schemes and Numerical Simulation

XIAO MIN DONG,[1,2]* MIAO YU,[2] ZUSHU LI,[3] CHANGRONG LIAO[2] AND WEIMIN CHEN[2]

[1]*State Key Laboratory of Mechanic Transmission, Chongqing University 400044 Chongqing, China*

[2]*College of Opto-Electronic Engineering, Key Lab of Optoelectronic Technology and System of Education Ministry, Chongqing University, Chongqing, China*

[3]*Automatic College of Chongqing University, 400044 Chongqing, China*

ABSTRACT: Due to significant nonlinearity of magnetorheological (MR) suspension, one of the main challenges in the application of this technology is to develop appropriate control algorithms. The main purpose of this study is to identify a suitable control method for semi-active isolation in MR suspension application. The semi-active control schemes include the following: a new proposed intelligent control scheme, Human Simulated Intelligent Control (HSIC) and three representative semi-active control schemes that are skyhook control, hybrid control algorithm, and fuzzy logic control. A full-car dynamic model considering the effect of roll motion is adopted as the baseline model for our analysis. After deriving the governing motion equations of the proposed dynamic model, the HSICler and other three controllers with nonlinearity of MR dampers are formulated. Then each control policy is applied to the baseline model equipped with four MR dampers. The performances of each control algorithm under various road conditions are compared along with the equivalent passive model in both time and frequency domains. The results indicate that the semi-active suspension with each control scheme is more effective than the passive in reducing vibration of the vehicle body. The results further indicate that HSICler performs the best among the considered control policies.

Key Words: magnetorheological, control, optimization.

INTRODUCTION

In recent years, research work on vibration suppression of a vehicle system using semi-active suspension has significantly increased. There are three broad classifications of suspension systems including passive, active, and semi-active. Each of these types of suspension has different advantages and disadvantages. Though the passive suspension system in common use provides design simplicity and cost effectiveness, performance limitations are inevitable due to the way its characteristics are optimized for given driving conditions, and do not perform well under normal driving conditions. On the other hand, the active suspension system can provide the best performance in a wide frequency range. However, active suspension systems are less commonly used than passive systems due to their associated cost and power requirements. Therefore, one way to resolve these problems is to adopt the semi-active suspension system. In principle, semi-active isolation systems can deliver the versatility, adaptability, and higher performance of active systems with a fraction of the power consumption. For the last decade, a very attractive and effective semi-active suspension system featuring magnetorheological (MR) fluids has been proposed by many researchers (Lee and Choi, 2000; Simon and Ahmadian, 2001; Lai and Liao, 2002; Yao et al., 2002; Liao and Wang, 2003; Sassi et al., 2005; Song et al., 2005; Karkoub and Zribi, 2006; Shen et al., 2006; Sahin et al., 2007). However, the nonlinear behavior of MR dampers makes it difficult to design effective semi-active control strategies, and consequently a wide range of control systems have been proposed in the literature.

In one of the first examinations of semi-active control, Karnopp et al. (1974) proposed a 'skyhook' damper control algorithm for a vehicle suspension system and demonstrated that this system offers improved performance over a passive system when applied to a single-degree-of-freedom system. To overcome the weakness of skyhook control in depressing the vibration of unsprung mass, Ahmadian and Simon (2002) and Ahmadian and Vahdati (2006) studied two others including groundhook control and hybrid control. The test results

*Author to whom correspondence should be addressed.
E-mail: xm_dong@126.com
Figures 1–5, 10 and 15–23 appear in color online: http://jim.sagepub.com

1045-389X/09/07 0771–16 $10.00/0 DOI: 10.1177/1045389X08099469

confirm the features of each control policy discussed in the past analytical studies. Skyhook control is much more effective in improving the ride comfort, groundhook control is effective in better road holding ability and improving vehicle stability, and hybrid control is a trade-off between skyhook and groundhook.

Besides the three well-known semi-active control strategies, some linear feedback control methods were also applied in vibration control of a suspension. Wang et al. (2003) proposed a PI control scheme for vibration attenuation of a quarter-vehicle model subject to idealized harmonic and transient base excitations, and Yamamoto and Nakano (2002) proposed a proportional feedback control of automotive suspension featuring electrorheological (ER) shock absorber. When these linear feedback control strategies were applied in engineering practice, they were limited since the significant nonlinearity, uncertainty, and time delay always exist in MR suspension systems.

To compensate for the nonlinearity of MR damper, many control techniques have been applied to control the MR suspension system. For example, Guo et al. (2004) proposed a neural network control to deal with the nonlinear hysteresis between its output force and relative velocity of MR damper in the MR suspension system. The method is proven effective in a low frequency range through numerical simulations and an experiment. Choi et al. (2002) proposed a H-infinity controller with inherent robustness against system uncertainties for a full-vehicle suspension system featuring MR dampers. The control performances are evaluated under various road conditions through the HILS methodology. The same control strategy was also proposed by Zribi and Karkoub (2004) and Du et al. (2005). Recently, many control methods including fuzzy logic control (Yagiz and Sakman, 2006; Yu et al., 2006), neural network-based fuzzy control (Eslaminasab et al., 2007), neuro-fuzzy control (Choi et al., 2001), discrete-time fuzzy sliding mode control (Sung et al., 2007), optimal fuzzy control (Wang and Hu, 2005), adaptive fuzzy logic control (Dong et al., 2006; Yang et al., 2006), etc. have been explored. Most of these studies used a quarter-car model or a half-car model through numerical simulation. All these efforts have proved that fuzzy logic control and its improvements are very popular for use in semi-active control, as they are very intuitive for the user, easily implemented, and can account for system nonlinearities. On the other hand, it can be seen that it is not an easy task to tune reasonable control rules.

In addition, theoretical and experimental researches have demonstrated that the performance of an MR suspension system is highly dependent on the choice of algorithm employed (Ying et al., 2003). Because the characteristics of the various semi-active devices are different (e.g., range of controllable MR fluids, response ability, etc.) and the semi-active control of MR suspension is highly nonlinear, a control algorithm that performs well for one device may not be suitable for use with another device.

Consequently, the main contribution of this work is to evaluate a selection of control algorithms for use in vehicle suspension system with four MR dampers. Four semi-active control algorithms are discussed, including the new intelligent control algorithm, Human Simulated Intelligent Control (HSIC) based on schema theory proposed in this study, skyhook control, hybrid control, and fuzzy logic control. In order to accomplish this goal, a cylindrical MR damper applicable for a middle-sized passenger vehicle is designed and manufactured. Then an experimentally verified polynomial model is used to simulate the behavior of the MR damper. After formulating the governing motion equations of full-car dynamic model considering the effect of roll, the HSICler is formulated and tuned by hybrid Taguchi genetic algorithm (Tsai et al., 2004). Three representative semi-active control algorithms including skyhook control, hybrid control, and fuzzy logic control are also developed on the basis of quarter-car MR suspension system. In numerical examples, the full-car dynamic model with four MR dampers is used to compare the performance of the proposed control algorithms. Control performances under bump and random road conditions with three vehicle velocities are presented in time and frequency domains. In addition, a comparative work between the HISC, skyhook control, hybrid control, and fuzzy logic control is undertaken by presenting control responses.

MR SUSPENSION SYSTEM

Fabrication of MR Damper

In this study, a cylindrical type of MR damper shown in Figure 1(a) is designed and manufactured. The MR damper works in mixed mode operation of valve mode and direct-shear mode. The MR damper is divided into the left and right chamber by the piston, and fully filled with the MR fluid. During the piston motion from the left to the right, the MR fluid flows through the gap between the inner cylinder and the piston. The magnetic field exists in the gap perpendicular to the motion direction of the MR fluid after the current is applied to the coil. The viscosity of the MR fluid in the gap is changed subjected to the magnet field and the pressure drop across the piston varies. Thus, the damping force of the MR damper is controllable by the intensity of the magnetic field. The diameter of the outer and inner cylinder is 50 and 48 mm, respectively. The compressed length of the MR damper is 330 mm. When it is extended, it reaches 508 mm. The dimensions of the MR damper have been determined by considering the geometry of the test car. Figure 1(b)

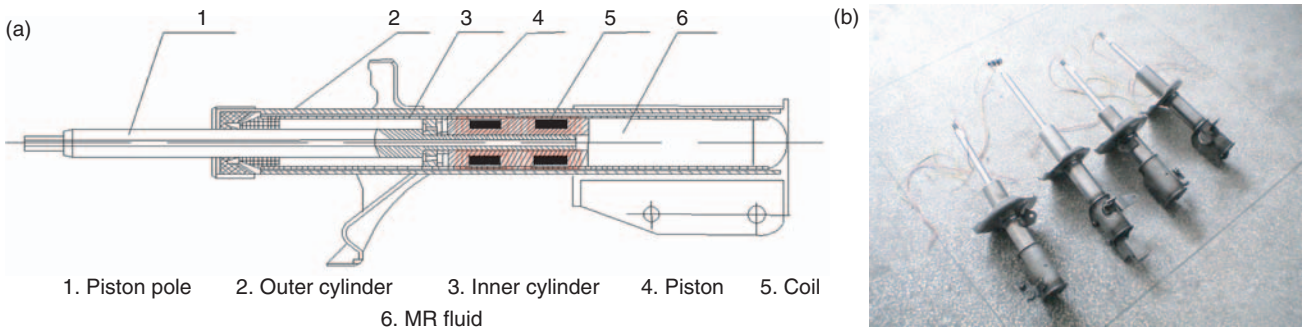

Figure 1. *The MR dampers of a passenger vehicle: (a) schematic configuration, (b) photograph of four MR dampers.*

shows the photograph of four MR dampers manufactured in this work.

In the absence of the magnetic field, the MR damper produces a damping force caused only by the fluid's viscous resistance. However, if a certain level of magnetic field is supplied to the MR damper, the MR damper produces an additional damping force owing to the yield stress of the MR fluid. This damping force of the MR damper can be continuously tuned by controlling the intensity of the magnetic field. To simplify the analysis of the damper, it is usually assumed that the MR fluids are incompressible and that the pressure in one chamber is uniformly distributed. Furthermore, it is assumed that the frictional force between oil seals and fluid inertia are negligible. Thus, the damping force of the MR damper can be given by Equation (1) based on the Bingham fluid model, flowing in the parallel duct, which is composed of velocity damping force and Coulomb friction (Yu et al., 2006):

$$F = -C_e V + F_{\mathrm{MR}} \tag{1}$$

in which $C_e = 24\eta A_p^2 l/bh^3 + 2\eta bl/h$, $F_{\mathrm{MR}} = -((4lA_{\mathrm{P}}/\eta) + 2bl)\tau_{\mathrm{y}}\mathrm{sgn}(V)$.

Experiment and Modeling of MR Damper

Although the damping force of MR damper can be easily computed by Equation (1) under a determined current, it is difficult to calculate the current inversely when the damping force is known since the relation of input current and damping force is highly nonlinear. Therefore, to evaluate the potential application of MR dampers, HSICler, and other three representative controllers in vibration control of MR suspension system, a model is developed to accurately reproduce the behavior of the MR damper and an experiment is set up to obtain the dynamic data necessary for identifying its model parameters.

The MR damper is measured by using the MTS in Figure 2. The MR damper is fixed between an upper and lower head on MTS test machine. The lower head is activated by the hydraulic cylinder up and down.

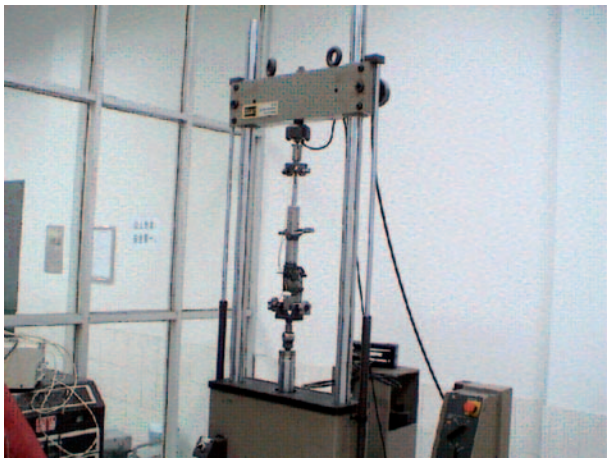

Figure 2. *MTS material testing system.*

The load cell on the upper head can record the force applied to the MR damper during tests. In each test, the hydraulic actuator drives the lower head with a varying sinusoidal displacement of fixed frequency and constant amplitude, and the input current to the MR damper is maintained at constant level, while the upper head is fixed. In this work, the excitation frequencies are 0.6369, 1.9108, and 3.8197 Hz and the displacement amplitudes are 25 mm, respectively, which present that the peak velocity of piston rod are 0.1, 0.3, and 0.6 m/s, respectively. The applied input current is from 0 to 2 A with increments of 0.4 A. The damper force is measured and recorded for plotting the characteristic of MR damper and constructing MR damper model. Velocity is obtained by differentiating the displacement. Figures 3(a) and (b) show the relation between damping force and piston rod displacement and the relation between damping force and piston rod velocity at peak velocity of 0.6 m/s under five different input currents for MR dampers of fore suspension.

The polynomial model is adopted in this study, which was first proposed by Choi et al. (2001), and provided a convenient and effective choice to calculate the desirable damper force in an open-loop control system. In this model, the hysteresis loop is divided into regions: positive acceleration (lower loop) and negative acceleration (upper loop), which can be fitted by the

polynomial with the power of piston velocity. Thus the damping force of the MR damper can be written:

$$f_{\mathrm{MR}} = \sum_{i=0}^{9} a_i v^i \quad i = 0, 1, \ldots, 9. \tag{2}$$

The efficient a_i can be linearly approximated with respect to the input current as follows: $a_i = b_i + c_i I$, $i = 0, 1, \ldots, 9$.

Therefore, the damping force can be expressed by:

$$f_{\mathrm{MR}} = \sum_{i=0}^{9} (b_i + c_i I) v^i. \tag{3}$$

The specific values of b_i and c_i used in this work are listed in Table 1.

To verify the obtained polynomial model, the measurement and simulation under four operating conditions are compared in Figure 4 with excitation frequency 3.8197 Hz and amplitude ±25 mm. Once the piston velocity is known and the desired force determined by control strategy, the control current is determined from Equation (4):

$$I = \frac{f_{\mathrm{MR}} - \sum_{i=0}^{6} b_i v^i}{\sum_{i=0}^{7} c_i v^i}. \tag{4}$$

Full Vehicle Dynamic Model

A full-car model with four MR dampers is shown in Figure 5. The vehicle body itself is assumed to be rigid and has degrees of freedom in heave, pitch, and roll directions. The governing equation of the full vehicle is derived as follows:

$$m_{\mathrm{s}} \ddot{z} = F_{\mathrm{fl}} + F_{\mathrm{fr}} + F_{\mathrm{rl}} + F_{\mathrm{rr}} \tag{5}$$

$$\left[I_{xx} + m_{\mathrm{s}} \left(\frac{H_c}{\cos\theta} \right)^2 \right] \ddot{\theta} = \frac{w}{2} F_{\mathrm{fl}} - \frac{w}{2} F_{\mathrm{fr}} + \frac{w}{2} F_{\mathrm{rl}} - \frac{w}{2} F_{\mathrm{rr}} + m_{\mathrm{s}} g \left(\frac{H_c}{\cos\theta} \right) \sin\theta + M_x \tag{6}$$

$$I_{yy} \ddot{\varphi} = a F_{\mathrm{fl}} + a F_{\mathrm{fr}} - b F_{\mathrm{rl}} - b F_{\mathrm{rr}} \tag{7}$$

$$m_{\mathrm{ufl}} \ddot{z}_{\mathrm{ufl}} = -F_{\mathrm{fl}} - k_{\mathrm{tfl}} (z_{\mathrm{ufl}} - z_{\mathrm{rfl}}) \tag{8}$$

$$m_{\mathrm{ufr}} \ddot{z}_{\mathrm{ufr}} = -F_{\mathrm{fr}} - k_{\mathrm{tfr}} (z_{\mathrm{ufr}} - z_{rfr}) \tag{9}$$

$$m_{\mathrm{url}} \ddot{z}_{\mathrm{url}} = -F_{\mathrm{rl}} - k_{\mathrm{trl}} (z_{\mathrm{url}} - z_{\mathrm{rrl}}) \tag{10}$$

$$m_{\mathrm{urr}} \ddot{z}_{\mathrm{urr}} = -F_{\mathrm{rr}} - k_{\mathrm{trr}} (z_{\mathrm{urr}} - z_{\mathrm{rrr}}) \tag{11}$$

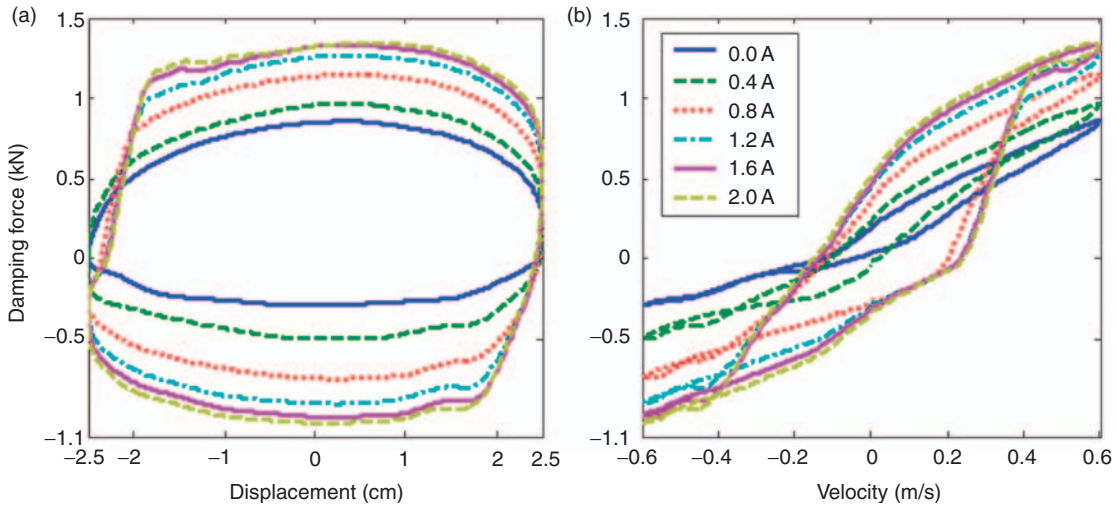

Figure 3. *Plots for damping force vs displacement and for damping force vs. velocity at peak velocity of 0.6 m/s.*

Table 1. Coefficients b_{fi} and c_{fi} of polynomial model.

Positive acceleration				Negative acceleration			
b_{f0}	−278.9883	c_{f0}	374.7905	b_{f0}	1113.47	c_{f0}	−534.6609
b_{f1}	−169.1461	c_{f1}	141.3833	b_{f1}	−314.50	c_{f1}	57.1168
b_{f2}	96.0680	c_{f2}	−261.3038	b_{f2}	−908.89	c_{f2}	478.9752
b_{f3}	83.4791	c_{f3}	−92.4920	b_{f3}	261.75	c_{f3}	−60.0778
b_{f4}	26.9841	c_{f4}	51.5936	b_{f4}	231.94	$c_{f4\mathrm{B}}$	−140.9436
b_{f5}	−0.9004	c_{f5}	14.9536	b_{f5}	−66.38	c_{f5}	20.9273
b_{f6}	−10.6079	c_{f6}	−2.6601	b_{f6}	−17.53	c_{f6}	14.4323
b_{f7}	−2.0571	c_{f7}	−0.1415	b_{f7}	3.82	c_{f7}	−2.7582
b_{f8}	1.3534	c_{f8}	1.0755	b_{f8}	0.86	c_{f8}	0.5481
b_{f9}	−0.1992	c_{f9}	−0.0606	b_{f9}	0.29	c_{f9}	0.0000

where:

$$F_{fl} = -k_{fl}(z_{fl} - z_{ufl}) - c_{fl}(\dot{z}_{fl} - \dot{z}_{ufl}) + F_{dfl},$$
$$F_{fr} = -k_{fr}(z_{fr} - z_{ufr}) - c_{fr}(\dot{z}_{fr} - \dot{z}_{ufr}) + F_{dfr},$$
$$F_{rl} = -k_{rl}(z_{rl} - z_{url}) - c_{rl}(\dot{z}_{rl} - \dot{z}_{url}) + F_{drl},$$
$$F_{rr} = -k_{rr}(z_{rr} - z_{urr}) - c_{rr}(\dot{z}_{rr} - \dot{z}_{urr}) + F_{drr}.$$

and:

$$z_{fl} = z - w\sin\theta - a\sin\varphi \approx z - w\theta - a\varphi,$$
$$z_{fr} = z + w\sin\theta - a\sin\varphi \approx z + w\theta - a\varphi,$$
$$z_{rl} = z - w\sin\theta + a\sin\varphi \approx z - w\theta + a\varphi,$$
$$z_{rl} = z + w\sin\theta + a\sin\varphi \approx z + w\theta + a\varphi,$$

in which:

$$F_{fl} = -k_{fl}(z_{fl} - z_{ufl}) - c_{fl}(\dot{z}_{fl} - \dot{z}_{ufl}) + F_{dfl},$$
$$F_{fr} = -k_{fr}(z_{fr} - z_{ufr}) - c_{fr}(\dot{z}_{fr} - \dot{z}_{ufr}) + F_{dfr},$$
$$F_{rl} = -k_{rl}(z_{rl} - z_{url}) - c_{rl}(\dot{z}_{rl} - \dot{z}_{url}) + F_{drl},$$
$$F_{rr} = -k_{rr}(z_{rr} - z_{urr}) - c_{rr}(\dot{z}_{rr} - \dot{z}_{urr}) + F_{drr},$$
$$z_{fl} = z - w\sin\theta - a\sin\varphi \approx z - w\theta - a\varphi,$$
$$z_{fr} = z + w\sin\theta - a\sin\varphi \approx z + w\theta - a\varphi,$$
$$z_{rl} = z - w\sin\theta + a\sin\varphi \approx z - w\theta + a\varphi,$$
$$z_{rl} = z + w\sin\theta + a\sin\varphi \approx z + w\theta + a\varphi.$$

Thus, the control damping force vector can be described as $u = [-c_{fl}(\dot{z}_{fl} - \dot{z}_{ufl}) + F_{dfl}, -c_{fr}(\dot{z}_{fr} - \dot{z}_{ufr}) + F_{dfr}, -c_{rl}(\dot{z}_{rl} - \dot{z}_{url}) + F_{drl}, -c_{rr}(\dot{z}_{rr} - \dot{z}_{urr}) + F_{drr}]^T$, which is determined by the below-discussed control strategies. Once the control input vector u is determined, the input current vector to be applied to the MR damper is obtained by Equation (4).

DESIGN OF HSICLER

The HSIC theory aims at emulating human behavior based on the human macro-control structure, and starts with the lowest level of hierarchical intelligent control, constructing the model of the 'motor sensory preview intelligence' in manual control. Thus, the theory possesses some excellent control properties like an expert operator. The original HSIC algorithm, first proposed by Prof. Zhou and others in 1983, has made big progress in recent years. The theory has been applied successfully in many perplexing processes and plants (such as delay system, multivariable system, nonlinear system, etc.). For example, Li and Wang (2003) have solved the swinging-up control of the single pendulum under limited torque with HSIC method.

The HSIC is a multilevel hierarchical structure information processing system with two levels in this study. As the lowest level of HSIC, the running control level, executes real-time control, based on the characteristic mode of a car, the motion attitudes of vehicle are identified and corresponding control means are selected

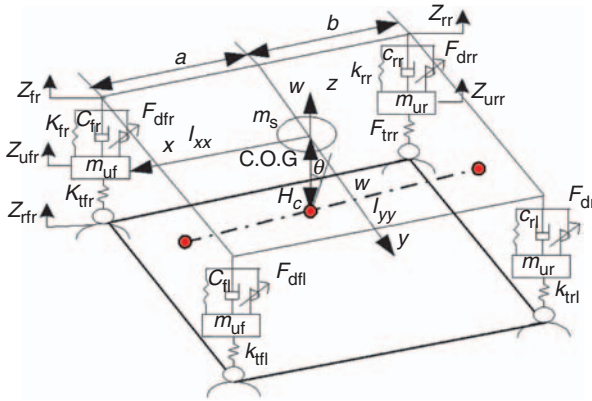

Figure 5. *Mechanical model of the MR suspension system.*

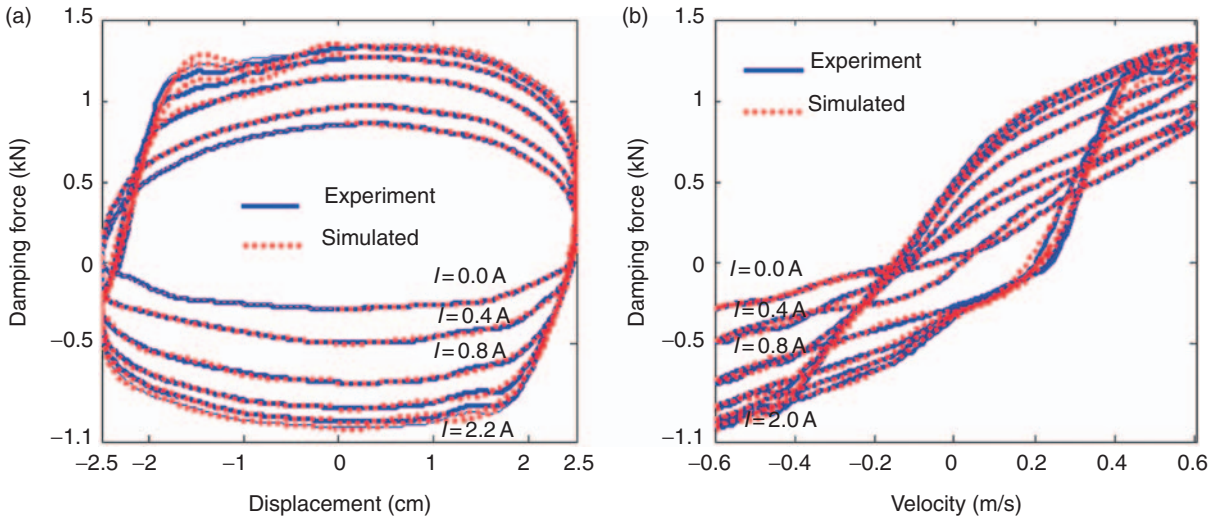

Figure 4. *Comparison of polynomial model and experimental results (3.8197 Hz, 25 mm): (a) force vs displacement; (b) force vs velocity.*

from among a combination of open-loop control, skyhook control and proportional plus differential control schemes. Assuming the vehicle body is rigid, the motion attitude of vehicle body consists one or more of heave, pitch, and roll motions. As a result, motion attitudes of running car can be classified eight kinds in Figure 6. After analyzing these attitudes, the first motion attitude is an ideal attitude with little change of motion attitude, which means good ride comfort and stability can be achieved; it is thus feasible to propose an open-loop control strategy. The second to eighth motion attitude are the coupling of one or more motion of heave, pitch, or roll motions owing to road input or driver's maneuvers. It is effective to propose to combine skyhook control with proportional plus differential control schemes.

At the second level, the parameter correction level, automatic readjustment of control mode parameters in running control level enhance the adaptability of HSIC. Both levels combined form a unit controller with structure of typical high-order production system. For each level in HSIC, the control problem solving is in reality a combination of qualitative and quantitative double mapping information process and decision procedure. The procedure of designing the intelligent control algorithm is the process of setting up a characteristic model and multimode control model. It can be described by production rule in the form of IF <condition> THEN <result> (condition is characteristics and result is decision). The two-level designs will be discussed in turn.

Running Control Level

At this level, eight sensor-motor intelligent schemas (SMIS) are designed to directly control corresponding attitudes according to the characteristic mode. Each SMIS consists of sensed schema, motion schema, and association schema. The design course of the eighth motion attitude including heave, pitch, and roll motions is similar to others. Therefore, only the design of eighth motion attitude is discussed in the following.

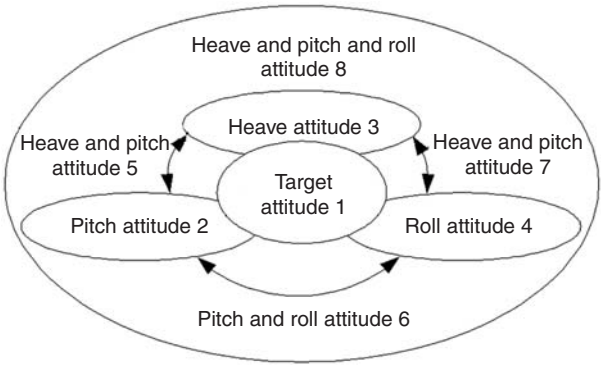

Figure 6. *Attitudes of a running car.*

SENSED SCHEMA

To determine the motion attitude of running car, a characteristic set can be selected:

$$S_{P8} = (R_8, Q_8, K_8, \otimes, \Phi) \tag{12}$$

in which $R_8 \in \sum^{14}, Q_8 \in \sum^{9}, K_8 \in \sum^{8\times 9}, \Phi_5 \in \sum^{8}$.

A characteristic primitive set is selected to effectively percept attitudes of running car and can be expressed as:

$$\begin{aligned} Q_8 = \Big\{ & q_{81}||z|>\delta_z, |\theta|>\delta_\theta, |\varphi|>\delta_\varphi, q_{82}|z\dot{z} \\ & <0, q_{83}|z\dot{z}\geq 0, q_{84}|\theta\dot{\theta}<0, q_{85}|\theta\dot{\theta} \\ & \geq 0, q_{86}|\varphi\dot{\varphi}<0, q_{87}|\varphi\dot{\varphi}\geq 0 \Big\}. \end{aligned} \tag{13}$$

The association matrix K_8 can be determined deflecting from or approaching the target attitude:

$$K_8 = \begin{pmatrix} 1 & 1 & 1 & 1 & 0 & 1 & 0 & 1 & 0 \\ 1 & 1 & 1 & 0 & 1 & 1 & 0 & 1 & 0 \\ 1 & 1 & 1 & 1 & 0 & 0 & 1 & 1 & 0 \\ 1 & 1 & 1 & 0 & 1 & 0 & 1 & 1 & 0 \\ 1 & 1 & 1 & 1 & 0 & 1 & 0 & 0 & 1 \\ 1 & 1 & 1 & 0 & 1 & 1 & 0 & 0 & 1 \\ 1 & 1 & 1 & 1 & 0 & 0 & 1 & 0 & 1 \\ 1 & 1 & 1 & 0 & 1 & 0 & 1 & 0 & 1 \end{pmatrix}.$$

As a result, the sensed characteristic model can be obtained:

$$\Phi_8 = K_8 \otimes Q_8$$

$$= \begin{Bmatrix} \phi_{81}||z|>\delta_z, |\theta|>\delta_\theta, |\varphi|>\delta_\varphi, z\dot{z}<0, \varphi\dot{\varphi}<0, \theta\dot{\theta}<0, \\ \phi_{82}||z|>\delta_z, |\theta|>\delta_\theta, |\varphi|>\delta_\varphi, z\dot{z}\geq 0, \varphi\dot{\varphi}<0, \theta\dot{\theta}<0, \\ \phi_{83}||z|>\delta_z, |\theta|>\delta_\theta, |\varphi|>\delta_\varphi, z\dot{z}<0, \varphi\dot{\varphi}\geq 0, \theta\dot{\theta}<0, \\ \phi_{84}||z|>\delta_z, |\theta|>\delta_\theta, |\varphi|>\delta_\varphi, z\dot{z}\geq 0, \varphi\dot{\varphi}\geq 0, \theta\dot{\theta}<0, \\ \phi_{85}||z|>\delta_z, |\theta|>\delta_\theta, |\varphi|>\delta_\varphi, z\dot{z}<0, \varphi\dot{\varphi}<0, \theta\dot{\theta}\geq 0, \\ \phi_{86}||z|>\delta_z, |\theta|>\delta_\theta, |\varphi|>\delta_\varphi, z\dot{z}\geq 0, \varphi\dot{\varphi}<0, \theta\dot{\theta}\geq 0, \\ \phi_{87}||z|>\delta_z, |\theta|>\delta_\theta, |\varphi|>\delta_\varphi, z\dot{z}<0, \varphi\dot{\varphi}\geq 0, \theta\dot{\theta}\geq 0, \\ \phi_{88}||z|>\delta_z, |\theta|>\delta_\theta, |\varphi|>\delta_\varphi, z\dot{z}\geq 0, \varphi\dot{\varphi}\geq 0, \theta\dot{\theta}\geq 0, \end{Bmatrix}. \tag{14}$$

MOTION SCHEMA

$$S_{M8} = (R_8, P_8, L_8, \Psi_8, U_8) \tag{15}$$

where, $P_8 \in \sum^{8}, L_8 \in \sum^{8\times 8}, \Psi_8 \in \sum^{8}$.

The eighth motion attitude involves heave, pitch, and roll motion. The control inputs are adjustable damping force of four MR dampers. Therefore, it is reasonable to independently calculate the damping force required by heave, pitch, and roll motion, respectively.

According to sensed schema, the heave motion can be classified in two situations. One is when car body closes to the target place, and skyhook control strategy is proposed:

$$F_{\mathrm{dfl}} + F_{\mathrm{dfr}} + F_{\mathrm{drl}} + F_{\mathrm{drr}} = -k_{\mathrm{sky}} C_{\mathrm{sky}-z} \dot{z}. \quad (16)$$

The other is when car body departs from the target place, and proportional plus differential control scheme is proposed:

$$F_{\mathrm{dfl}} + F_{\mathrm{dfr}} + F_{\mathrm{drl}} + F_{\mathrm{drr}} = -k_{\mathrm{pd}}(K_{\mathrm{p}-z} z + K_{\mathrm{d}-z} \dot{z}). \quad (17)$$

To restrain pitch motion, we can get similar equations. When car body closes to the target place:

$$-F_{\mathrm{dfl}} a - F_{\mathrm{dfr}} a + F_{\mathrm{drl}} b + F_{\mathrm{drr}} b = -k_{\mathrm{sky}} C_{\mathrm{sky}-\varphi} \dot{\varphi}. \quad (18)$$

When car body departs from target place:

$$-F_{\mathrm{dfl}} a - F_{\mathrm{dfr}} a + F_{\mathrm{drl}} b + F_{\mathrm{drr}} b = -k_{\mathrm{pd}}(K_{\mathrm{p}-\varphi} \varphi + K_{\mathrm{d}-\varphi} \dot{\varphi}). \quad (19)$$

With the same principle, the damping forces to restrain roll motion can also be calculated as following respectively:

$$F_{\mathrm{dfl}} \frac{w}{2} - F_{\mathrm{dfr}} \frac{w}{2} + F_{\mathrm{drl}} \frac{w}{2} - F_{\mathrm{drr}} \frac{w}{2} = -k_{\mathrm{sky}} C_{\mathrm{sky}-\theta} \dot{\theta} \quad (20)$$

$$F_{\mathrm{dfl}} \frac{w}{2} - F_{\mathrm{dfr}} \frac{w}{2} + F_{\mathrm{drl}} \frac{w}{2} - F_{\mathrm{drr}} \frac{w}{2} = -k_{\mathrm{pd}}(K_{\mathrm{p}-\theta} \theta + K_{\mathrm{d}-\theta} \dot{\theta}). \quad (21)$$

It is impossible to calculate the four damping forces through three equations. If neglecting the torsion of car body, an equation can be supplemented:

$$F_{\mathrm{dfl}} \frac{w}{2} - F_{\mathrm{dfr}} \frac{w}{2} - F_{\mathrm{drl}} \frac{w}{2} + F_{\mathrm{drr}} \frac{w}{2} = 0. \quad (22)$$

According to sensed schema, an equation group consists of (15), (16), (19), and (21) or (16), (18), (20), and (21). The equation group is resolved to get a control force vector $p_1 = (F_{\mathrm{dfl}}, F_{\mathrm{dfr}}, F_{\mathrm{drl}}, F_{\mathrm{drr}})^T$.

ASSOCIATION SCHEMA

$$\Omega_8 = \Phi_8 \to \Psi_8, \Omega_8 \quad \{\omega_{11}, \omega_{12}, \ldots, \omega_{18}\} \quad (23)$$

where ω_{8j}: IF φ_{8j} THEN ψ_{8j} $(j = 1, \ldots, 8)$.

Therefore, the whole schema of the eighth attitude can be written as:

$$S_{KG,8} = \langle S_{P,8}, S_{M,8}, S_{A,8} \rangle. \quad (24)$$

After the other seven schemas of running level are formulated, all schemas, including all sensed schemas, all motion schemas, and all associated schemas, can be described together.

The all sensed schema is:

$$S_P = (R,\ Q,\ K,\ \otimes,\ \Phi) \quad (25)$$

in which, $R \in \sum^{14}, Q \in \sum^{6}, K \in \sum^{8\times 6}, \Phi \in \sum^{8}$.

The characteristic primitive set is:

$$Q = \Big[q_1 || z| > \delta_z, q_2 || \theta| > \delta_\theta, q_3 || \varphi| > \delta_\varphi, q_4 || z| \le \delta_z, q_5 || \theta| \le \delta_\theta, q_6 || \varphi| \le \delta_\varphi \Big]^T. \quad (26)$$

Finally the associated matrix is:

$$K = \begin{pmatrix} 0 & 0 & 0 & 1 & 1 & 1 \\ 1 & 0 & 0 & 0 & 1 & 1 \\ 0 & 1 & 0 & 1 & 0 & 1 \\ 0 & 0 & 1 & 1 & 1 & 0 \\ 1 & 0 & 1 & 0 & 1 & 0 \\ 0 & 1 & 1 & 1 & 0 & 0 \\ 1 & 1 & 0 & 0 & 0 & 1 \\ 1 & 1 & 1 & 0 & 0 & 0 \end{pmatrix}$$

As a result, characteristic mode set can be determined:

$$\Phi = K \otimes Q = \Big\{ \phi_1 || z| \le \delta_z, .|\theta| \le \delta_\theta, |\varphi| \le \delta_\varphi, \phi_2 || z| > \delta_z, |\theta| \le \delta_\theta, |\varphi| \le \delta_\varphi \phi_3 || z| \le \delta_z, |\theta| > \delta_\theta, |\varphi| \le \delta_\varphi, \phi_4 || z| \le \delta_z, |\theta| \le \delta_\theta, |\varphi| > \delta_\varphi, \phi_5 || z| > \delta_z, |\theta| \le \delta_\theta, |\varphi| > \delta_\varphi, \phi_6 || z| \le \delta_z, |\theta| > \delta_\theta, |\varphi| > \delta_\varphi, \phi_7 || z| > \delta_z, |\theta| > \delta_\theta, |\varphi| \le \delta_\varphi, \phi_8 || z| > \delta_z, |\theta| > \delta_\theta, |\varphi| > \delta_\varphi \Big\}. \quad (27)$$

The all motion schema is:

$$S_M = (R,\ P,\ L,\ \Psi,\ U) \quad (28)$$

where, $P \in \sum^{8}, L \in \sum^{8\times 8}, \Psi \in \sum^{8}$

The control mode primitive set is:

$$P = \Big\{ S_{KG,1}, S_{KG,2}, S_{KG,3}, S_{KG,4}, S_{KG,5}, S_{KG,6}, S_{KG,7}, S_{KG,8} \Big\}. \quad (29)$$

If the mode computing matrix is $L = I_{8\times 8}$, the control mode set can be obtained:

$$\Psi = L \cdot P^T. \quad (30)$$

The all associated schema is:

$$S_A = \{\Omega : \Phi \to \Psi\},$$
$$\Omega = \{\Omega_1, \Omega_2, \Omega_3, \Omega_4, \Omega_5, \Omega_6, \Omega_7, \Omega_8\} \quad (31)$$
$$\Omega_j : \text{IF } \Phi_j \text{ THEN } \Psi_j \ (j = 1, 2, \ldots, 8).$$

Consequently, all SMIS of running level for MR suspension system can be concluded:

$$S_{KG} = \langle S_P, S_M, S_A \rangle. \quad (32)$$

Parameter Adjustment Level

To increase adaptive ability of HSIC, two adjustable factors k_{sky} and k_{pd} are introduced in running control level. The adjusting rule can be written:

IF $\text{RMS}(a) < \text{RMS}(a_0)$

$$k_{\text{sky}} = \frac{\text{RMS}(a_s)}{\text{RMS}(a_0)} \quad (33)$$

ELSE

$$k_{\text{pd}} = \frac{\text{RMS}(a_s)}{\text{RMS}(a_0)}. \quad (34)$$

The Structure of HSIC based on SMIS

The HSICler based on SMIS with two levels with hierarchical structure is shown in Figure 7. In this figure, the MR semi-active suspension system is excited by road. The HSICler consists of two levels: the running level and parameter adjustment level. At the top level, the parameter adjustment level adaptively modifies control parameters when the running road condition is changed. At running level, eight SMISes automatically switch according the condition of running car. One fundamental SMIS of running level can be described as double mapping relation in Figure 8.

In Figure 8, the control mode ψ is not fixed and a function of open-loop hold control, skyhook, or PD control. The control output vector can be calculated through Figure 9.

The Parameters of HSICler are Determined by Hybrid Taguchi Genetic Algorithm

Some threshold parameters of HSICler that need to be determined initially are $C_{\text{sky}-z}$, $C_{\text{sky}-\varphi}$, $C_{\text{sky}-\theta}$, $K_{\text{p}-z}$, $K_{\text{p}-\varphi}$, $K_{\text{p}-\theta}$, $K_{\text{d}-z}$, $K_{\text{d}-\varphi}$, and $K_{\text{d}-\theta}$; the others such as K_{sky} and K_{pd} can be adjusted at parameter adjustment level while running. Usually, the course of determination for those threshold value parameters need much trial and error. Therefore, in this article, a HTGA (Tsai et al., 2004) is proposed to tune the parameters through the Matlab 6.5\Simulink full-car model that is responsible for generating the root mean square of accleration of vehicle.

ENCODING AND INITIALIZATION OPERATION

The real number encoding is adopted in this article. The length of chromosome is determined by the number of the threshold parameters. If $(x_1, x_2, \ldots, x_i, \ldots, x_9)$ is the optimal solution, the initialization chromosomes can be obtained by:

$$x_i = l_i + \beta(u_i - l_i). \quad (35)$$

FITNESS FUNCTION

To choose the ideal threshold value parameters, a trade-off is assumed between ride comfort and stability. Therefore, the fitness function is chosen as:

$$\text{Fitness}(t) = \alpha\text{RMS}(\ddot{z}) + \beta\text{RMS}(\ddot{\theta}) + \gamma\text{RMS}(\ddot{\varphi}) + \sum_{i=f,j=l}^{r,r} \omega_{ij}\text{RMS}(\ddot{z}_{uij}). \quad (36)$$

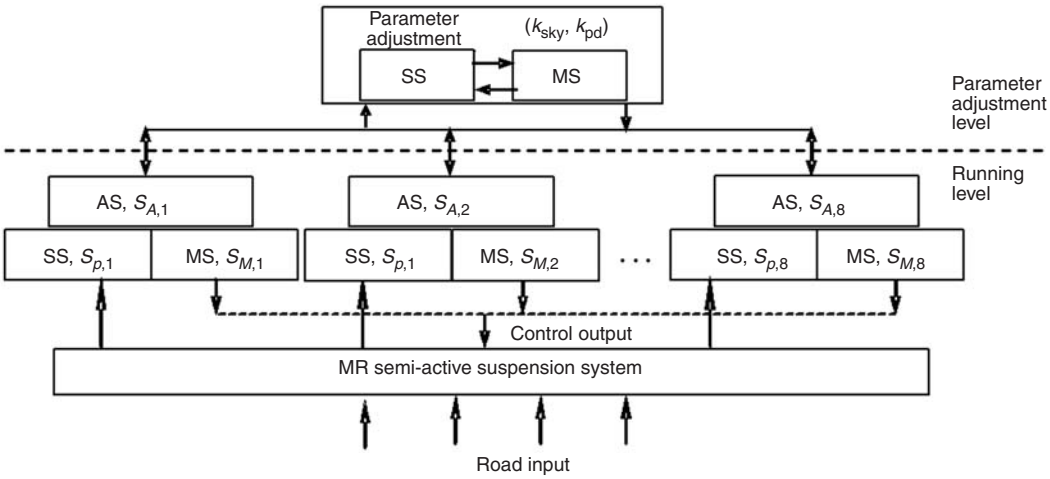

Figure 7. *HSICler for MR suspension.*

In this study, $\alpha = 0.4, \beta = 0.2, \gamma = 0.1$, $\omega_{fl} = \omega_{fr} = \omega_{rl} = \omega_{rr} = 0.075$.

CROSSOVER AND MUTATION

The crossover operators used here are one-cut-point crossover by convex crossover. After generation of diverse offspring by crossover operation, the orthogonal arrays of Taguchi method are used to study the nine parameters of HSIC controller with a small number of experiments (Figure 10). In this work, a two-level orthogonal array $L_{12}(2^{11})$ is used. The $L_{12}(2^{11})$ represents 12 columns and 11 individual experiments corresponding to 11 rows; only the first nine columns are used, and the other two columns are ignored. The best level for each gene is determined from two chromosome chosen randomly at each run by orthogonal experiments with 16 times. Once the optimal level of each gene is selected, one can obtain the optimal chromosomes.

The mutation operator used in this article is convex combination. The parameters used in the simulation of the HTGA are population size = 150, mutation probability = 0.3, crossover probability = 0.1. After 100 generations, the optimized parameters are shown in Table 2.

FORMULATION OF THREE REPRESENTATIVE CONTROL SCHEMES

So far, a variety of approaches have been proposed in the literature for the control of semi-active suspension. As comparison of HSICler, three model-free semi-active control algorithms have been formulated, including skyhook control, hybrid control, and fuzzy logic control. To develop the three controllers, the popular quarter-car model is adopted and derived from the full-car model in Figure 5. A full-car model consists of four independent quarter-car models corresponding to four corners of full vehicle, respectively. Therefore, four independent controllers need to be designed. Taking fore left suspension model as an example, the three representative controllers are formulated in the following.

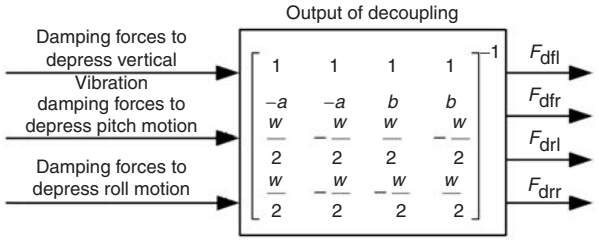

Figure 9. *The generating course of control mode.*

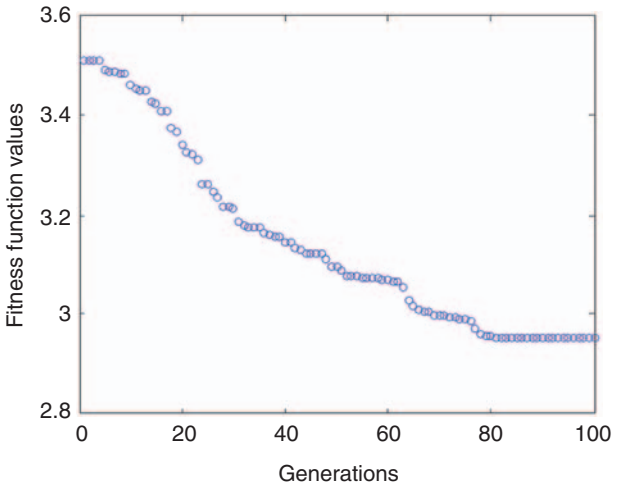

Figure 10. *Convergence trends of fitness function values.*

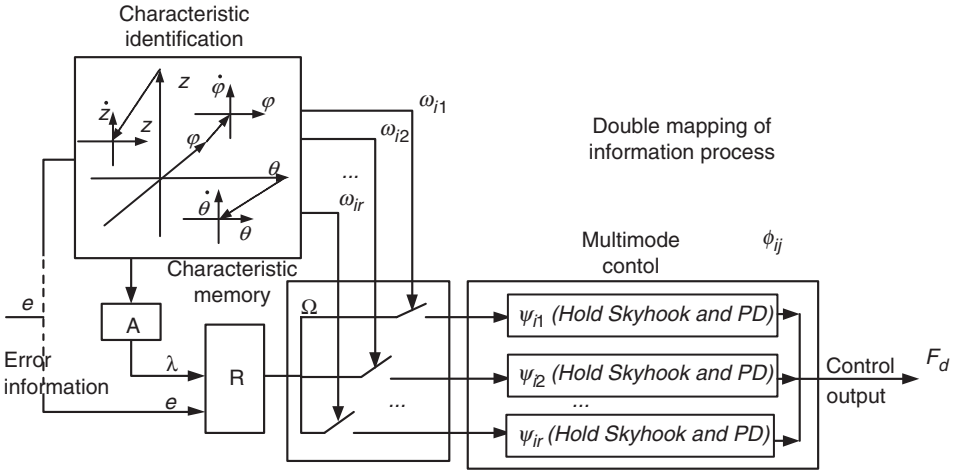

Figure 8. *Double mapping relation of HSIC in control and decision.*

Table 2. Initial parameters and optimized parameters.

	C_{sky-z}	K_{p-z}	K_{d-z}	$C_{sky-\varphi}$	$K_{p-\varphi}$	$K_{d-\varphi}$	$C_{sky-\theta}$	$K_{p-\theta}$	$K_{d-\theta}$
Initial parameters	2000	1000	1500	1000	700	750	1000	500	750
Lower limit	1000	750	1000	800	500	500	800	300	500
Upper limit	4000	2000	3000	2000	1500	1500	1500	1500	1500
Optimized parameters	3210.0	1324.2	2515.1	1400.0	842.5	1210.7	1311.4	756.3	1058.5

Skyhook Damping Control

As a classical semi-active control approach, skyhook damping control was first proposed by Karnopp in 1973. The control strategy is adopted widely to control semi-active suspension through numerical and experimental research. The approach supposes the sprung body is connected to a virtual sky by a damper. The skyhook control law is mathematically described by:

$$F_{dfl-sky} = \begin{cases} G_{sky}\dot{z}_{fl} & \dot{z}_{fl}(\dot{z}_{fl}-\dot{z}_{ufl})>0 \\ 0 & \dot{z}_{fl}(\dot{z}_{fl}-\dot{z}_{ufl})\le 0 \end{cases}. \quad (37)$$

Hybrid Control

The hybrid control approach is a combination of a skyhook control approach and a groundhook control law. The goal of hybrid control approach is to provide direct control of both the sprung and unsprung bodies. Ahmadian et al. studied the control policy (2002, 2006). The results indicated that hybrid control could offer benefit to both the sprung mass and the unsprung.

If the groundhook control law can be written as:

$$F_{dfl-ground} = \begin{cases} -G_{ground}\dot{z}_{ufl} & \dot{z}_{ufl}(\dot{z}_{fl}-\dot{z}_{ufl})\le 0 \\ 0 & \dot{z}_{ufl}(\dot{z}_{fl}-\dot{z}_{ufl})>0 \end{cases}. \quad (38)$$

Then the equation for hybrid control law is:

$$F_{dfl-hybrid} = \alpha F_{dfl-sky} - (1-\alpha)F_{dfl-ground}. \quad (39)$$

Fuzzy Logic Control

Due to nonlinearity and uncertainty of MR suspension, fuzzy logic control independent of model is also adopted. It is switchable for real-time application because of these reasons. The idea of fuzzy logic control imitates human intelligence in the learning and decision-making process. Instead of using very tedious digital manipulations, fuzzy logic adopts linguistic variables or human languages to describe the quantity and measurement, and to classify them in terms of levels. In this study, a fuzzy logic control algorithm is employed to design a controller for vibration isolation and to compare with others.

The sprung mass velocity $\dot{z}_{sfl}$, unsprung mass velocity $\dot{z}_{usfl}$, and relative velocity $(\dot{z}_{sfl}-\dot{z}_{usfl})$ between them are the input variables of the fuzzy controller while the damping force F_{dfl} is its output. A_i, B_j, C_k $(i, j, k = 1–5)$ are the fuzzy subsets of three input variables (V_{sfl}, V_{ufl}, V_{relfl}) with value (NB, NS, ZE, PS, PB). Their membership functions figure is shown in Figures 11 and 12. The fuzzy subset of output variables is U_n $(n = 1–5)$ with value (NB, NM, NS, ZE, PS, PM, PB). The fuzzy control rules (shown in Tables 3 and 4) are based on skyhook and groundhook strategies in order to improve ride comfort without sacrificing driving stability.

Execution of rules in Table 3:

$$R_l^1 = A_i \times U_n \cap B_j \times U_n = R_{Al}^1 \cap R_{Bl}^1, \quad (i,j,n = 1,2,\ldots,5, \quad l = 1,2,\ldots,25). \quad (40)$$

Execution of rules in Table 4:

$$R_l^2 = C_i \times U_n \cap B_j \times U_n = R_{Cl}^2 \cap R_{Bl}^2, \quad (i,j,n = 1,2,\ldots,5, \quad l = 1,2,\ldots,25). \quad (41)$$

For one input (V_{sfl0}, V_{relfl0}, V_{ufl0}), controlled variables are executed by rules in Table 3:

$$U_{sfll} = V_{sfl0} \circ R_{Al}^1 \cap V_{relfl0} \circ R_{Bl}^1, \quad l = 1,2,\ldots,25 \quad (42)$$

$$U_{sfl} = \bigvee_{l=1}^{25} U_{sfll}, \quad l = 1,2,\ldots,25. \quad (43)$$

Controlled variables are executed by rules in Table 4:

$$U_{ufll} = V_{ufl0} \circ R_{Cl}^2 \cap V_{relfl0} \circ R_{Bl}^2, \quad l = 1,2,\ldots,25 \quad (44)$$

$$U_{ufl} = \bigvee_{l=}^{25} U_{ufll}. \quad (45)$$

The defuzzification used for this research is the weighted average method. The last controller output is given by Equation (46):

$$F_{dfl} = K\frac{\alpha\sum_{n=1}^{7}\mu_{U_n}(U_{sfl})\cdot U_n + (1-a)\sum_{n=1}^{7}\mu_{U_n}(U_{ufl})\cdot U_n}{\alpha\sum_{n=1}^{7}\mu_{U_n}(U_{sfl})\cdot U_n + (1-a)\sum_{n=1}^{7}\mu_{U_n}(U_{ufl})} \quad (46)$$

where K is output factor, α is adjust factor, and $0 \le \alpha \le 1$.

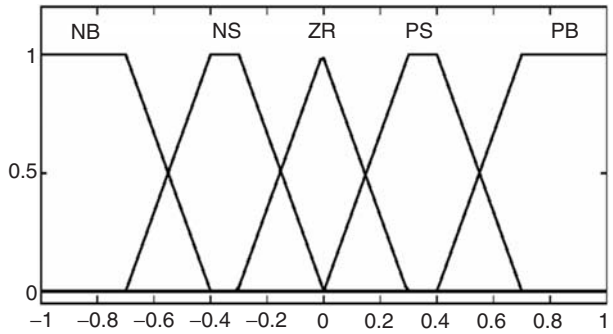

Figure 11. *Input membership function.*

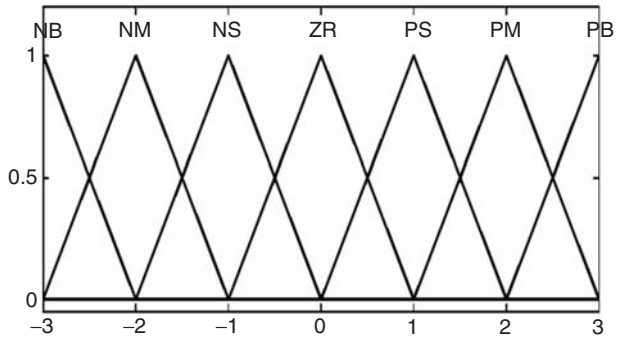

Figure 12. *Output membership function.*

Table 3. Control rules based on skyhook.

V_s \ V_{rel}	NB	NS	ZE	PS	PB
NB	PB	PM	PS	ZE	ZE
NS	PM	PS	ZE	ZE	ZE
ZE	PM	PS	ZE	NS	NM
PS	ZE	ZE	ZE	NS	NM
PB	ZE	ZE	NS	NM	NB

Table 4. Control rules based on groundhook.

V_u \ V_{rel}	NB	NS	ZE	PS	PB
NB	ZE	ZE	PS	PM	PB
NS	ZE	ZE	ZE	PS	PM
ZE	NM	NS	ZE	PS	PM
PS	NM	NS	ZE	ZE	ZE
PB	NB	NM	NS	ZE	ZE

An adaptive adjustor is designed to correct the output force in real time. The performance of semi-active suspension will be optimal by continuous modification and feedback. If n is the number of samples and T is sampling interval, then controller output sequence can be given as follows:

$$F'_{\mathrm{dfl}}(nT) = F_{\mathrm{dfl}}(nT) + m \times Y(nT), \quad m \in [0, 1] \qquad (47)$$

where $Y(nT)$ is correction matrix that is obtained by self-learning online; m is a factor of proportionality.

NUMERICAL SIMULATION AND RESULTS

In this section, the performance of the semi-active output feedback of the above four controllers applied to the full-vehicle dynamic mode with four MR damper is evaluated. The nominal model parameters for full-car model are shown in Table 5.

Once the desirable damper force is obtained according to the above designed controllers, the control of input current to achieve the desirable damper force is determined from Equation (4), where the desired damper force vector F_d to be tracked is set by the motion schema in Equation (15), skyhook control damping force in Equation (37), hybrid control damping force in Equation (39), or fuzzy logic control damping force in Equation (46), respectively, then applied to the MR dampers. Due to the actual constraint of the input current to the MR damper, the input current is restricted within 0 and 1.5 A in this study. The block diagram for the semi-active controllers of full-vehicle model with four MR dampers is depicted in Figure 13. It can be seen that the desired damper forces are calculated from the designed controllers, which are equal to the active control force, then this desired force is approximately realized by the MR damper with an appropriate input current using Equation (4).

In order to equally evaluate the four semi-active control policies, the proposed HTGA above is also applied to tune the control gains of the three representative control strategies. Consequently, G_{sky} equals 2540 Ns/m, G_{ground} equals 2830 Ns/m, a equals 0.73.

Now, to validate the control performance characteristics of above four control strategies, numerical simulation of the full-car suspension system under various roads and vehicle speeds are carried out in MATLAB and SIMULINK using a fourth order Rung–Kutta integration scheme. The numerical conditions consist of bump road at speed of 30 km/h, and both B class road and D class road at speed of 40, 60, and 80 km/h. The dimensions of bump road are determined by measuring the actual speed bump in Figure 14. The random road inputs of two fore wheels have the road power spectral density (Zhao and Lu, 1999):

$$G_{x_r}(n) = G_{x_r}(n_0)\left(\frac{n}{n_0}\right)^{-w}. \qquad (48)$$

If the vehicle velocity is v_0, then the delay time of the rear wheel excitations compared to fore wheel excitations is

Table 5. Simulation parameters of saloon car.

Parameter	Value	Parameter	Value	Parameter	Value
m_s	745.2 kg	k_{fl}, k_{fr}	30,000 N/m	$k_{tfl}, k_{tfr}, k_{trl}, k_{trr}$	181,000 N/m
I_{xx}	375.2 kgm^2	k_{rl}, k_{rr}	32,500 N/m	c_{fl}, c_{fr}	1039.7 N/m/s
I_{yy}	768.8 kgm^2	w	1.277 m	c_{rl}, c_{rr}	2638.0 N/m/s
m_{ufl}, m_{ufr}	25.35 kgm^2	a	1.1161 m	H_c	0.37 m
m_{url}, m_{urr}	68.8 kgm^2	b	1.2319 m		

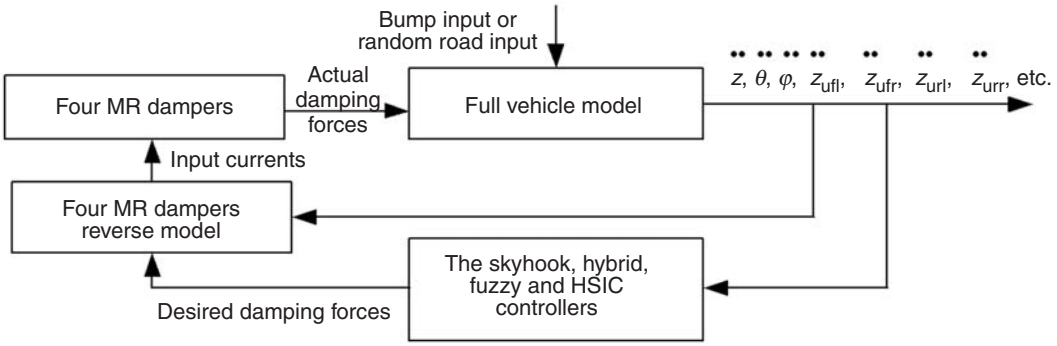

Figure 13. *Block diagram of semi-active controllers for full vehicle suspension model with four MR dampers.*

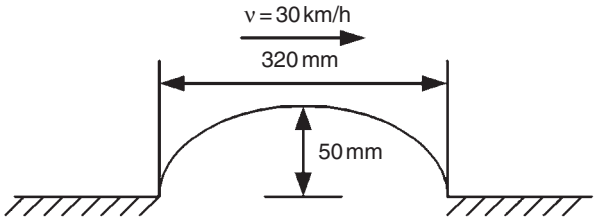

Figure 14. *Speed bump excitation profile.*

$\Delta t = l/v_0 = (a+b)/v_0$. Thus, the time serials of four wheels road model with D class road at speed of 80 km/h via simulation are shown in Figure 15 according to Equation (48).

In this study, the characterization in terms of acceleration would be an appropriate index for four control schemes, since the human body or sprung mass is sensitive to inertial forces. The ratio of the root mean square (RMS) reduction of the response acceleration using control scheme to the RMS of the response acceleration with passive suspension system is used as a performance index to evaluate the comparison of vibration isolation performance. This is defined by:

$$TR = \frac{\mathrm{RMS}(\ddot{x}_{\mathrm{pass}}) - \mathrm{RMS}(\ddot{x}_{\mathrm{semi}})}{\mathrm{RMS}(\ddot{x}_{\mathrm{pass}})} \times 100\%. \qquad (49)$$

The time histories of vehicle body vertical acceleration and pitch angular acceleration under bump input at vehicle speed of 30 km/h are shown in Figures 16 and 17. Some peak-to-peak values including heave acceleration, pitch angular acceleration, fore suspension deflection, and rear suspension deflection are given in Table 6.

It is well-known that the first peak-to-peak acceleration value has great influence on a human's ride comfort when a car runs across a speed bump. To evaluate the responses under the speed bump input, the ration of peak-to-peak acceleration reduction with four semi-active control schemes to the peak-to-peak acceleration with passive suspension system is calculated in Table 6. In this table, a positive percentage means performance improvement is achieved, whereas a negative percentage denotes performance is worsened. It can be seen that the MR suspension with four designed controllers can depress the peak-to-peak vertical or angular acceleration compared with passive one. However, the MR suspension system with four designed controllers will degrade the suspension deflection. Among the four designed control strategies, the first peak-to-peak acceleration of the MR suspension with HSICler is reduced by over 25% compared with passive ones.

In addition, the responses of the sprung mass acceleration and unsprung mass acceleration are shown in Figures 18 and 19. For brevity, only the responses of the acceleration power spectral density

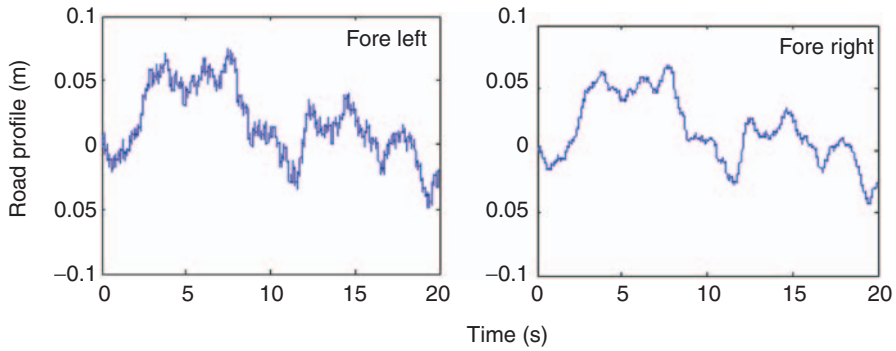

Figure 15. *The random road input time serials of two fore wheels.*

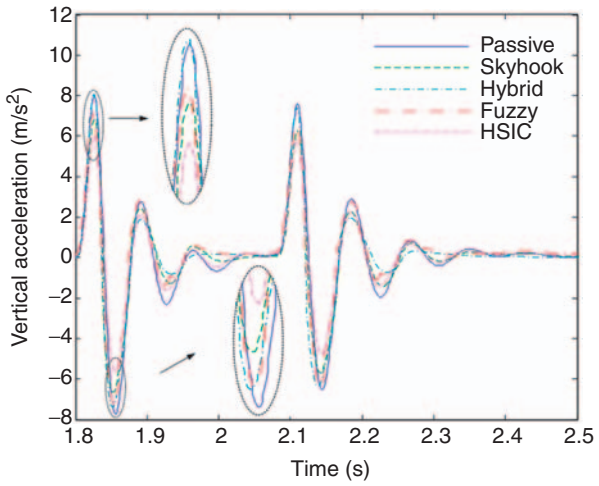

Figure 16. *The time history of vertical acceleration of body under bump input at vehicle speed of 30 km/h.*

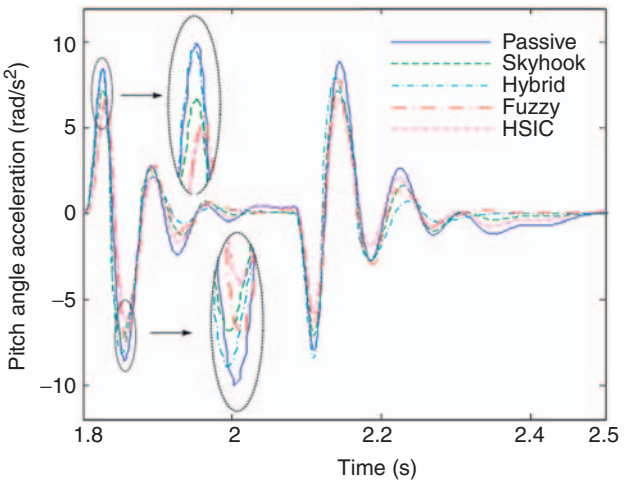

Figure 17. *The pitch angular acceleration time history of body under bump input at vehicle speed of 30 km/h.*

(PSD) at speed of 80 km/h on B class road are presented. Other root-mean-square (RMS) values of the responses are given in Figures 20–23 considering the frequency weighting from 0 to 50 Hz. It can also be seen that the semi-active suspension systems via all the four control strategies have good performance in sprung mass acceleration, pitch angular acceleration, and roll angular acceleration compared to that of passive suspension system. Noteworthy, the semi-active suspensions with fuzzy logic controller, hybrid controller or HSICler will also improve the performance of unsprung mass but not the skyhook controller in Figures 18 and 19. Considering the human sensitive frequency range 4–8Hz, the semi-active suspension system via HSICler can achieve the best improvement in ride comfort of all four designed controllers. On the other hand, the semi-active suspension system with HSICler can only have a moderate effect on depressing the vibration of tire compared with that with fuzzy logic controller.

When the vehicle speed is increased, the vibration of vehicle becomes more violent. Compared to passive suspension system, the semi-active suspension system with all four controllers can also depress the vibration of vehicle body. The semi-active suspension system with skyhook controller or hybrid controller will degrade the performance of unsprung mass except for that with fuzzy logic controller or HSICler. Of all four designed controllers, the HSICler can achieve the best ride comfort and stability. When the road is changed from class B road to class D road, results similar to those on class B road can be achieved.

CONCLUSION

In this study, a new model-free control algorithm is proposed based on full-vehicle dynamic model. Together with three represented model-free semi-active control algorithms that are formulated, all four designed controllers are applied to the full-vehicle MR suspension model with four MR dampers. The polynomial model of MR damper is constructed through the experimental data.

Table 6. Comparison of control performance under speed bumps.

	Peak-to-peak value of heave acceleration (%)	Peak-to-peak value of pitch angular acceleration (%)	Peak-to-peak value of fore suspension deflection(%)	Peak-to-peak value of rear suspension deflection(%)
Skyhook	14.40	14.95	−7.17	−4.34
Hybrid	1.70	3.10	−2.93	−3.14
Fuzzy	7.34	15.82	−3.95	−1.35
HSIC	25.01	25.00	−3.95	−1.65

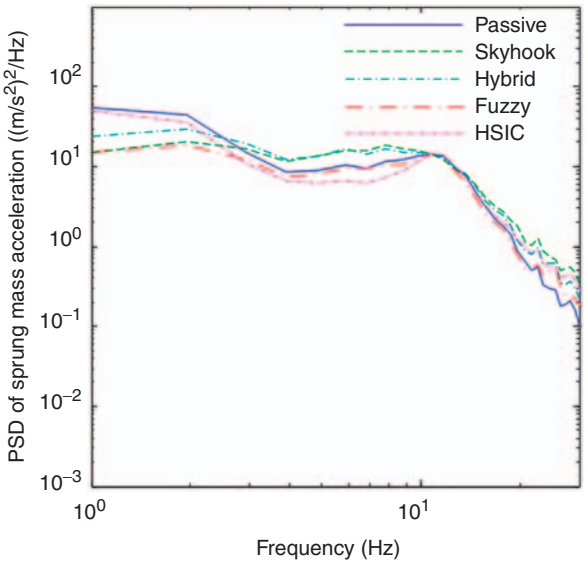

Figure 18. *The PSD of sprung mass acceleration under bump input at vehicle speed of 80 km/h on B class road.*

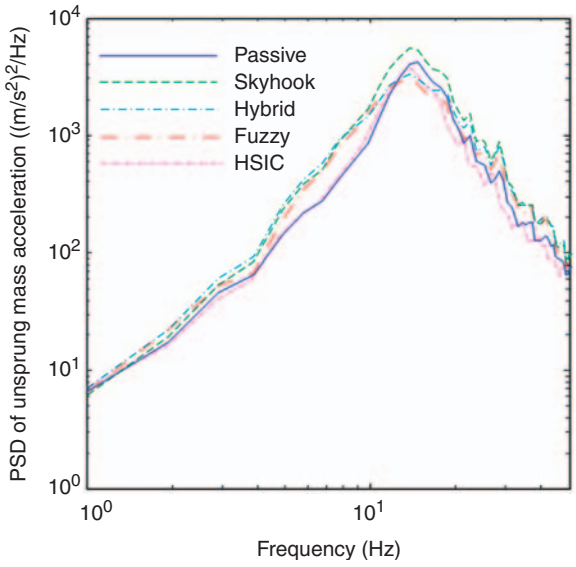

Figure 19. *The PSD of unsprung mass acceleration under bump input at vehicle speed of 80 km/h on B class road.*

The performances of all the four designed controllers are validated and compared by numerical simulation on various road conditions and vehicle speeds. The results demonstrate that the performances of the

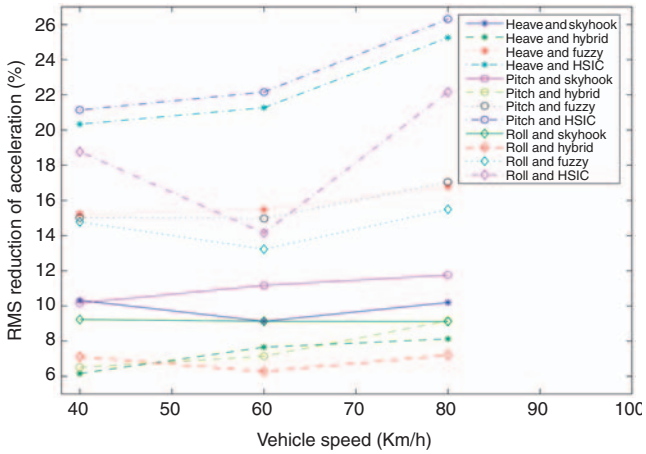

Figure 20. *The vibration acceleration reduction comparison of vehicle body on B class road.*

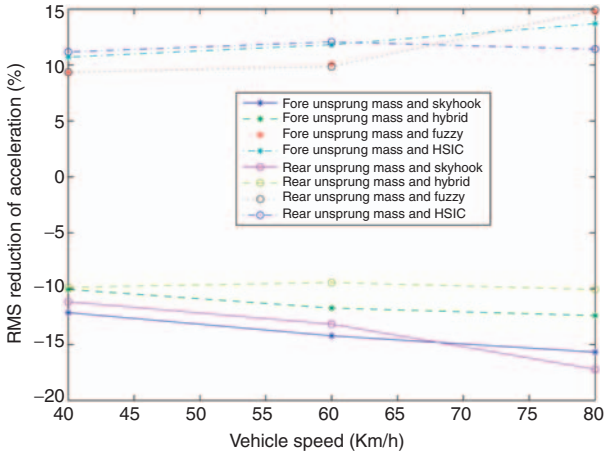

Figure 21. *The vibration acceleration reduction comparison of fore or rear suspension unsprung mass on B class road.*

resulting controlled system are highly dependent on the control algorithm employed. Each controller performed noticeably better than the passive controllers in some way. As for bump input, the peak-to-peak acceleration values are achieved with HSICler. Under random road, HSICler can also achieve great improvement of ride comfort and stability. In a word, the semi-active suspension system with HSICler exhibits better comprehensive properties. The next paper will examine issues related to actual road test

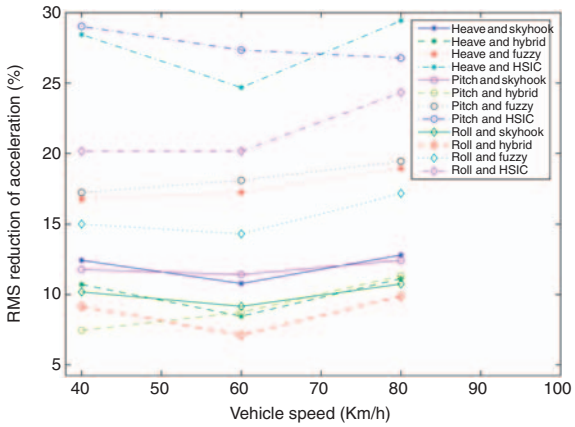

Figure 22. *The vibration reduction acceleration comparison of vehicle body on D class road.*

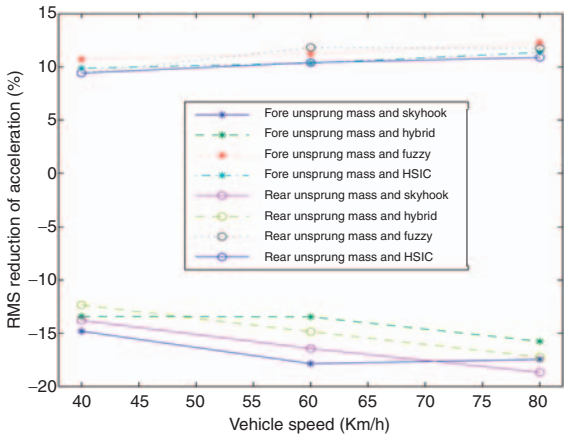

Figure 23. *The vibration acceleration reduction comparison of fore or rear suspension unsprung mass on D class road.*

and the robustness analysis of those semi-active control algorithms.

NOMENCLATURE

A_P = effective piston area
R_l = inner radius of the cylinder
h = width of damping path
l = length of damping path
η = viscosity of MR fluid
τ_y = yield stress caused by the applied magnetic field
b_i, c_i = coefficient obtained from the fitness of experimental data
I = MR damper input current
f_{MR} = the desired damping force determined by control strategy.
$z_{fl}, z_{fr}, z_{rl}, z_{rr}$ = fore left suspension spring mass displacement, fore right suspension spring displacement, rear left suspension spring mass displacement, rear right suspension spring mass displacement
m_s = sprung mass
$m_{ufl}, m_{ufr}, m_{url}, m_{urr}$ = unsprung mass of fore left suspension, fore right suspension, rear left suspension, rear right suspension
I_{xx}, I_{yy} = roll and pitch mass moment of inertia
$k_{fl}, k_{fr}, k_{rl}, k_{rr}$ = spring constants of the suspensions
$.k_{tfl}, k_{tfr}, k_{trl}, k_{trr}$ = stiffness coefficients of the tires
$z_{fl}, z_{fr}, z_{rl}, z_{rr}$ = vertical displacements of four corners of vehicle body
$z_{ufl}, z_{ufr}, z_{url}, z_{urr}$ = vertical displacements of unsprung mass
z, θ, φ = heave displacement, pitch and roll angular displacement
$z_{rfl}, z_{rfr}, z_{rrl}, z_{rrr}$ = road excitations
a, b = distance between the front damper and center of gravity (CG) of sprung mass, distance between the rear damper and CG of sprung mass
$c_{fl}, c_{fr}, c_{rl}, c_{rr}$ = invariable damping coefficients of four MR dampers
$F_{dfl}, F_{dfr}, F_{drl}, F_{drr}$ = controllable damping forces of four MR dampers
$\delta_z, \delta_\theta, \delta_\varphi$ = threshold values
k_{sky} = skyhook damping coefficient modification factor
$C_{sky-z}, C_{sky-\varphi}, C_{sky-\theta}$ = skyhook damping coefficient
k_{pd} = proportional differential control modification factor
$K_{p-z}, K_{p-\varphi}, K_{p-\theta}$ = proportional factor
$K_{d-z}, K_{d-\varphi}, K_{d-\theta}$ = differential factor
RMS(a_s), RMS(a_0) = root mean square vertical acceleration of car body during a period of time
a_0 = reference vertical acceleration of car on B grade road at 60 km/h.
β = a random number and $\beta \in \{0.1, 0.2, 0.3, \ldots, 1\}$
x_i = initialization chromosomes
u_i, l_i = upper limit and lower limit of x_i
a = weighting factor
T = simulation time
$F_{dfl-sky}$ = skyhook damping force
$\dot{z}_{fl}$ = sprung mass velocity of fore left MR suspension
$\dot{z}_{ufl}$ = unsprung body velocity
G_{sky} = skyhook gain
G_{ground} = groundhook gain
$F_{dfl-sky}$ = skyhook damping force
$F_{dfl-ground}$ = groundhook damping force
$\ddot{x}_{pass}$ = RMS of acceleration of passive suspension system
$\ddot{x}_{semi}$ = RMS of acceleration of MR suspension system

ACKNOWLEDGMENTS

We would like to thank the authors of the references for their clarification. This research is supported financially by the National Natural Science Foundation of People's Republic of China (Project No. 60574074 No. 60804018, and No. 60404014), the Post-doctoral Fund of People's Republic of China (No. 20070420719), and the Chongqing Natural Science Foundation (CSTC. 2008BB6184). This support is gratefully acknowledged.

REFERENCES

Ahmadian, M. and Simon, D.E. 2002. "An Analytical and Experimental Evaluation of Magneto Rheological Suspensions for Heavy Trucks," *Vehicle System Dynamics*, 37:38–49.

Ahmadian, M. and Vahdati, N. 2006. "Transient Dynamics of Semiactive Suspensions with Hybrid Control," *Journal of Intelligent Material Systems and Structures*, 17(2):145–153.

Choi, S.B., Lee, H.S. and Park, Y.P. 2002. "H-infinity Control Performance of a Full-vehicle Suspension Featuring Magnetorheological Dampers," *Vehicle System Dynamics*, 38(5):341–360.

Choi, S.B., Suh, M.S., Park, D.W. and Shin, M.J. 2001. "Neuro-fuzzy Control of a Tracked Vehicle Featuring Semi-active Electro-rheological Suspension units," *Vehicle System Dynamics*, 35(3):141–162.

Dong, X.M., Yu, M., Liao, C.R., Chen, W.M., Zhang, H.H. and Huang, S.L. 2006. "Adaptive Fuzzy Neural Network Control for Transient Dynamics of Magneto-rheological Suspension with Time-delay," *Advances in Neural Networks - Isnn 2006, Pt 2, Proceedings* 3972:1046–1051.

Du, H.P., Sze, K.Y. and Lam, J. 2005. "Semi-active H-infinity Control of Vehicle Suspension with Magneto-rheological Dampers," *Journal of Sound and Vibration*, 283(3–5):981–996.

Eslaminasab, N., Biglarbegian, M., Melek William W. and Gorlanraghi, M.F. 2007. "A Neural Network Based Fuzzy Control Approach to Improve Ride Comfort and Road Handling of Heavy Vehicles using Semi-active Dampers," *International Journal of Heavy Vehicle Systems*, 14(2):135–157.

Guo, D.L., Hu, H.Y. and Yi, J.Q. 2004. "Neural Network Control for a Semi-active Vehicle Suspension with a Magnetorheological Damper," *Journal of Vibration and Control*, 10(3):461–471.

Karkoub, M.A. and Zribi, M. 2006. "Active/Semi-active Suspension Control using Magnetorheological Actuators," *International Journal of Systems Science*, 37(1):35–44.

Karnopp, D.C., Crosby, M.J., and Harwood, R.A. 1974. "Vibration Control using Semi-active Force Generators," *ASME Journal of Engineering for Industry*, 96(2):619–626.

Lai, C. Y. and Liao, W. H. 2002. "Vibration Control of a Suspension System via a Magnetorheological Fluid Damper," *Journal of Vibration and Control*, 8(4):527–547.

Lee, H.S. and Choi, S.B. 2000. "Control and Response Characteristics of a Magneto-rheological Fluid Damper for Passenger Vehicles," *Journal of Intelligent Material Systems and Structures*, 11(1):80–87.

Li, Z. and Wang, G. 2003. "Schema Theory and Human Simulated Intelligent Control," In: *Proceedings of the 2003 IEEE on Robotics & intelligent Systems and Signal Processing, Changsha, China, October*, pp. 524–530.

Liao, W.H. and Wang, D.H. 2003. "Semiactive Vibration Control of Train Suspension Systems via Magnetorheological Dampers," *Journal of Intelligent Material Systems and Structures*, 14(3):161–172.

Sahin, H., Liu, Y., Wang, X., Gordaninejad, F., Evrensel, C. and Fuchs, A. 2007. "Full-scale Magnetorheological Fluid Dampers for Heavy Vehicle Rollover," *Journal of Intelligent Material Systems and Structures*, 18(12):1161–1167.

Sassi, S., Cherif, K., Mezghani, L., Thomas, M. and Kotrane, A. 2005. "An Innovative Magnetorheological Damper for Automotive Suspension: From Design to Experimental Characterization," *Smart Materials & Structures*, 14(4):811–822.

Shen, Y., Golnaraghi, M.F. and Heppler, G.R. 2006. "Semi-active Vibration Control Schemes for Suspension Systems using Magnetorheological Dampers," *Journal of Vibration and Control*, 12(1):3–24.

Simon, D. and Ahmadian, M. 2001. "Vehicle Evaluation of the Performance of Magneto Rheological Dampers for Heavy Truck Suspensions," *Journal of Vibration and Acoustics – Transactions of the ASME*, 123(3):365–375.

Song, X.B., Ahmadian, M. and Southward, S. 2005. "An Adaptive Semiactive Control Algorithm for Magnetorheological Suspension Systems," *Journal of Vibration and Acoustics-Transactions of the ASME*, 127(5):493–502.

Sung, K.G., Han, Y.M., Lim K.H. and Choi, S.B. 2007. "Discrete-time Fuzzy Sliding Mode Control for a Vehicle Suspension System Featuring an Electrorheological Fluid Damper," *Smart Materials and Structures*, 16(3):798–808.

Tsai, J.-T., Liu, T.-K. and Chou, J.-H. 2004. "Hybrid Taguchi-genetic Algorithm for Global Numerical Optimization," *IEEE Transaction on Evolutionary Computer*, 8(4):365–377.

Wang, E.R., Ma, X.Q., Rakheja, S. and Su, C.Y. 2003. "Semi-active Control of Vehicle Vibration with MR-dampers," In: *Proceedings of the 42nd IEEE Conference on Decision and Control*, Maui, Hawaii, USA.

Wang, H. and Hu, H.Y. 2005. "Optimal Fuzzy Control of a Semi-active Suspension of a Full-vehicle Model using MR Dampers," *International Journal of Modern Physics B*, 19(7–9):1513–1519.

Yagiz, N. and Sakman, L.E. 2006. "Fuzzy Logic Control of a Full Vehicle Without Suspension Gap Degeneration," *International Journal of Vehicle Design*, 42(1–2):198–212.

Yamamoto, H. and Nakano, M. 2002. "Rheological Properties and Dynamic Mechanical Model of a Magnetorheological Suspension in Pressure Flow Mode," *Journal of the Society of Rheology*, Japan, 30(2):83–88.

Yang, J.W., Li, J. and Du, Y.P. 2006. "Adaptive Fuzzy Control of Lateral Semi-active Suspension for High-speed Railway Vehicle," *Computational Intelligence, Pt 2, Proceedings*, 4114: 1104–1115.

Yao, G.Z., Yap, F.F., Chen, G., Li, W.H. and Yeo, S.H. 2002. "MR Damper and its Application for Semi-active Control of Vehicle Suspension System," *Mechatronics*, 12(7):963–973.

Ying, Z.G., Zhu, W.Q. and Soong T.T. 2003. "A Stochastic Optimal Semi-active Control Strategy for ER/MR Damper," *Journal of Sound and Vibration*, 259(1):45–62.

Yu, M., Liao, C.R., Chen, W.M. and Huang, S.L. 2006. "Study on MR Semi-active Suspension System and its Road Testing," *Journal of Intelligent Material Systems and Structures*, 17(8–9):801–806.

Zhao, H. and Lu, S. 1999. "A Vehicle's Time Domain Model with Road Input on Four wheels," *Automotive Engineering*, 21(2):112–117.

Zhou, Q.J. and Bai, J.G. 1983. "An Intelligent Controller of Novel Design," In: *Proceedings of A Multi-national Instrument Conference, Part 1*, Shanghai, China, pp.137–149.

Zribi, M. and Karkoub, M. 2004. "Robust Control of a Car Suspension System using Magnetorheological Dampers," *Journal of Vibration and Control*, 10(4):507–524.